Advances in Concrete Construction, *Vol. 10, No. 1* (*2020*) *49-59*
DOI: https://doi.org/10.12989/acc.2020.10.1.049

Quasi-static test of the precast-concrete pile foundation for railway bridge construction

Xiyin Zhang*, Xingchong Chen, Yi Wang, Mingbo Ding, Jinhua Lu and Huajun Ma

School of Civil Engineering, Lanzhou Jiaotong University, 88 Anning West Road, Lanzhou, Gansu, 730070, China

(*Received February 25, 2020, Revised June 15, 2020, Accepted June 26, 2020*)

Abstract. Precast concrete elements in accelerated bridge construction (ABC) extends from superstructure to substructure, precast pile foundation has proven a benefit for regions with fragile ecological environment and adverse geological condition. There is still a lack of knowledge of the seismic behavior and performance of the precast pile foundation. In this study, a 1/8 scaled model of precast pile foundation with elevated cap is fabricated for quasi-static test. The failure mechanism and responses of the precast pile-soil interaction system are analyzed. It is shown that damage occurs primarily in precast pile-soil interaction system and the bridge pier keeps elastic state because of its relatively large cross-section designed for railways. The vulnerable part of the precast pile with elevated cap is located at the embedded section, but no plastic hinge forms along the pile depth under cyclic loading. Hysteretic curves show no significant strength degradation but obvious stiffness degradation throughout the loading process. The energy dissipation capacity of the precast pile-soil interaction system is discussed by using index of the equivalent viscous damping ratio. It can be found that the energy dissipation capacity decreases with the increase of loading displacement due to the unyielding pile reinforcements and potential pile uplift. It is expected to promote the use of precast pile foundation in accelerated bridge construction (ABC) of railways designed in seismic regions.

Keywords: railway bridge construction; precast concrete pile foundation; elevated pile cap; quasi-static test; seismic performance

1. Introduction

Precast bridge construction, also known as accelerated bridge construction (ABC, for short), offers many advantages over conventional construction and has been widely accepted all over the world (Hällmark *et al*. 2012, Wang *et al*. 2014, Shim *et al*. 2018, Titchenda Chan and Zachary 2020). Use of precast concrete elements in construction is a common strategy adopted in ABC, and the precast extends from bridge superstructure to substructure, such as pier column and pile foundation (Bu *et al*. 2012, Cheng and Sritharan 2019). Precast concrete piles have already been used for bridge foundations in US and Europe (Fam *et al*. 2003, Gould 2019, Dziadziuszko and Sobala 2018). Despite widespread application of the ABC, there is still a lack of knowledge of the behavior and performance of precast concrete elements during earthquakes. Once the earthquake happens, bridge piles will be subjected to large bending and shear forces together with axial loads of varying intensities due to the inertial and kinematic forces generated by loads and soil displacement (Thusoo *et al*. 2020). It is known that considerable loads from the superstructure must be transferred down through the substructure, through the pile cap into the piles, and then finally into the soils (Xiao *et al*. 2006). Therefore, the pile foundation is a critical link in the load transferring process of bridges during a seismic event.

The concern about the seismic performance of precast bridge elements limited the application of ABC in regions of high seismicity (Wang *et al*. 2008). Through existing experimental study, it has been verified that the bridge with precast elements have adequate seismic performance (Mashal and Palermo 2019). Large numbers of researches focus on the precast bridge piers or columns (Ou *et al*. 2010a, Ameli and Pantelides 2017, Tong *et al*. 2019, Do *et al*. 2019). While, it is also urgently needed to study the behavior and performance of precast pile foundation during earthquakes. In recent years, some researchers start to pay attention to precast bridge piles. Schmeisser and Benzoni (2008) developed a rational design methodology for precast, prestressed concrete piles, and used proven seismic design methodology and constitutive modeling to produce detailing requirements. Using an internet-based network platform, Xiao *et al*. (2012) investigated the seismic response of bridge pier and precast concrete pile foundation, and found that the sudden spalling of the thick concrete cover of the precast pile may cause unstable response of the bridge pier and pile foundation system under simulated earthquake loading. Kong *et al*. (2016) believed that the soils surrounding the precast pile have the most significant effects on the bridge responses, but they put emphasis on the integral abutment bridges.

Generally, cast-in-place construction of concrete bridges typically results in extensive damage to the onsite environment due to the land demand for construction activities (Ou *et al*. 2010a). Therefore, precast-concrete pile is suitable for regions with fragile ecological environment

*Corresponding author, Associate Professor
E-mail: zhangxiyin@mail.lzjtu.cn

ISSN: 2287-5301 (Print), 2287-531X (Online)

Fig. 1 Bridges with elevated-cap pile foundation along QTR (Qin and Zheng 2010, You *et al*. 2017)

and adverse geological condition, such as coastal soft soil region, collapsible loess region and permafrost region *et al*. Particularly in permafrost region, the elevated pile-cap foundation is always applied to reduce the thermal disturbance to permafrost (Qin and Zheng 2010, You *et al*. 2017, Zhang *et al*. 2017). Figure.1 shows the example of the bridges with elevated-cap pile foundation along Qinghai-Tibet railway (QTR) in China. Besides, the elevation of the cap can also bring great convenience and low cost to the bridge construction (Wang *et al*. 2016). Because the cast-in-place pile bring large hydration heat release from concrete (Liu *et al*. 2019b, Shang *et al*. 2018, Gao *et al*. 2019), use of precast pile foundation in permafrost region can minimize the thermal disturbance of construction to vulnerable permafrost.

For the elevated-cap pile embedded partially in soils may suffer large deflections under lateral loads, which make it difficult for them to remain in the elastic state (Blanco *et al*. 2019). It is not suitable for the capacity protection principle in current design codes (Chen *et al*. 2020). For the present, plastic hinge has been detected first at the top of the outer pile under cyclic loading, the position of the plastic hinge is shallower in pile foundation with larger aboveground height (Wang *et al*. 2016). However, most of these researches have been related to the elevated pile-cap foundation for highway bridges used in coastal regions or deep river. Limited attention has been paid to the railway bridges in regions without water area, just as shown in Fig. 1.

In order to minimize the negative impacts of bridge construction in regions with fragile ecological environment and adverse geological condition, such as permafrost region, it is expected to promote the use of precast pile foundation in accelerated bridge construction (ABC). Elevated cap is suitable for the precast pile foundation in these special regions. This study aims to investigate the failure mechanism and responses of the precast-concrete pile foundation with elevated cap under cyclic lateral loading. In consideration of the rapid development of

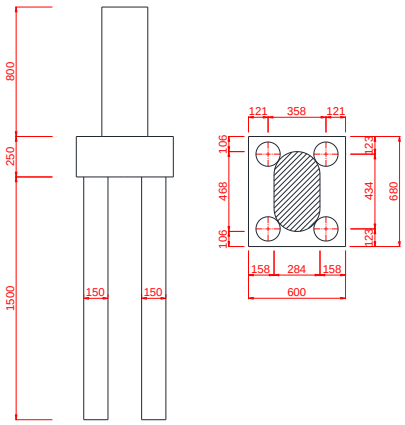

(a) Prototype structure

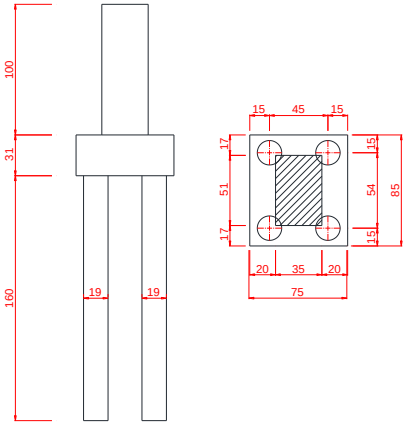

(b) scaled model

Fig. 2 Dimensions of the bridge pier with pile foundation (unit: cm)

railways in cold and quake-prone regions of Western China, the standard short-span bridge along Qinghai-Tibet railway is selected as protype. A 1/8 scaled model of bridge pier-pile-soil system is fabricated for quasi-static testing. Based on the test results, the cyclic behavior of the precast-concrete pile foundation with elevated cap is discussed for further seismic performance evaluation and seismic design.

2. Model design and fabrication

2.1 Model design

A type of pre-stressed T-shaped beam bridge widely used in Qinghai-Tibet railways is selected as the prototype in this study. The cube compressive strength of concrete is 30 MPa. The longitudinal reinforcement ratios of the bridge pier and pile are 0.40% and 0.43%, respectively. The railway bridge piers have low reinforcement ratio (less than 0.5%) in China (Lu *et al*. 2019). A 1/8-scaled model is designed for quasi-static testing based on the prototype bridge. To facilitate construction, the round-ended pier in prototype is simplified to rectangular section in the scaled model. Different from the cast-in-place construction in prototype, the pile foundation in scaled model will be replaced by the precast concrete element. Dimensions of the

Table 1 Similarity ratios of the physical quantities

C_σ	C_E	C_υ	C_η	C_c	C_φ	C_γ	C_P	C_u	C_L
1	1	1	1	1	1	1/L	L^2	L	L

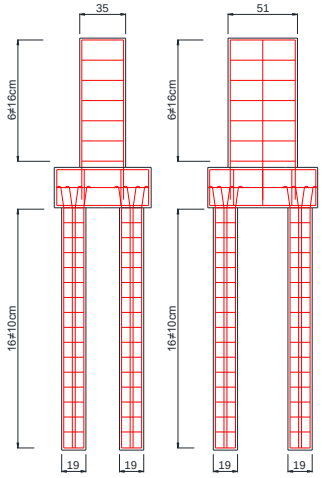

Fig. 3 Reinforcement arrangement of the model pier and piles

prototype and scaled model pier with pile foundation are shown in Figs. 2 (a) and (b), respectively.

In order to determine the configuration of the scaled model, dimensional analysis based on a generalized Π-theorem (Buckingham's Π-theorem) (Sonin 2004) is conducted. The lateral response can be determined by 10 physical quantities, i.e., normal stress σ, dimension L, concrete elasticity modulus E, concrete passion ratio υ, reinforcement ratio η, soil cohesive force c, soil internal friction angle φ, unite weight γ, external force P and displacement u. Take the similarity ratio of the normal stress σ as C_σ=1, then the similarity ratios of the other quantities are shown in Table 1. For the 1/8 scaled model, L is equal to 8.

According to the similarity theory and Table 1, except for the unit weight of concrete, the other material parameters of the scaled model are same to the prototype bridge (similarity ratio equals to 1). The increase of the unit weight of the scaled model can be considered by the additional weight during testing. The external force acted on the scaled model is $1/L^2$ times of the prototype and the lateral displacement is 1/L times of the prototype. Therefore, the concrete cube compression strength of the model pier, pile and pile cap is 30 MPa. Four longitudinal steel bars with a diameter of 6mm are used in the model pile, which constitutes a 0.4% steel ratio. The standard yield strength and ultimate strength of steel reinforcing bars used in the model pile are 300 Mpa and 420 Mpa, respectively. Six longitudinal steel bars with a diameter of 12 mm are used in model pier, which constitute a 0.38% steel ratio. The standard yield strength and ultimate strength of steel reinforcing bars used in the model pier are 335 Mpa and 455 Mpa, respectively. The reinforcement arrangement of the model pier and piles is shown in Fig. 3.

2.2 Model fabrication

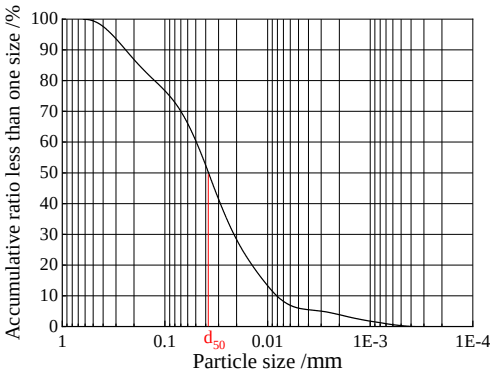

Fig. 4 Soil particle size distribution

(a) Steel banding (b) Concrete pouring

(c) Concrete curing

Fig. 5 Pile precasting process

The model fabrication sequence is as follows:

First is pile precasting; then are foundation soil packing and pile installation, the particle size distribution of the soil used in this study is shown in Fig. 4; and finally, the pile cap and pier are constructed in-situ.

(1) Pile precasting

Pile precasting includes the following procedures, as shown in Fig. 5.

(a) Steel banding: The longitudinal reinforcement and stirrups are assembled as a reinforcement skeleton frame. Strain gages are attached at the polished positions on longitudinal steel bars and sealed with glue to prevent failure.

(b) Concrete pouring: PVC pipes are used as concrete shuttering; vibration of concrete is carried out with an insertion-type vibrator during concrete pouring.

(c) Concrete curing: PVC pipes can be easily removed by cutting when the concrete strength reaches the specified strength target, then comes the longtime concrete curing (no less than 28 days).

(a) Pile planting (b) Soil compaction

(c) Device installation

Fig. 6 Soil packing and pile installation

(a) Concrete framework (b) Concrete pouring (c) Concrete curing

Fig. 7 Pier and pile cap construction

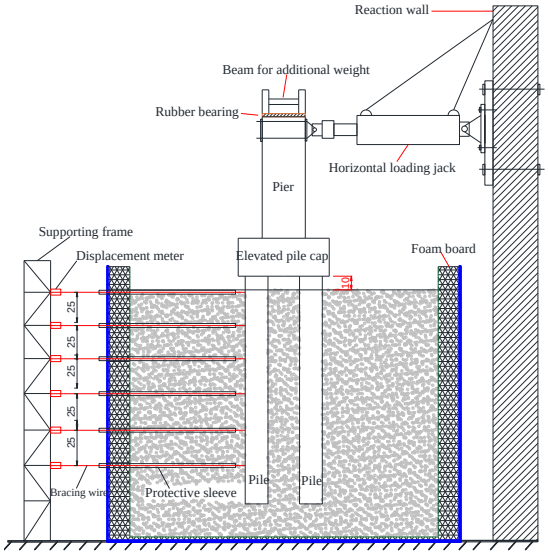

(a) Lateral loading unit

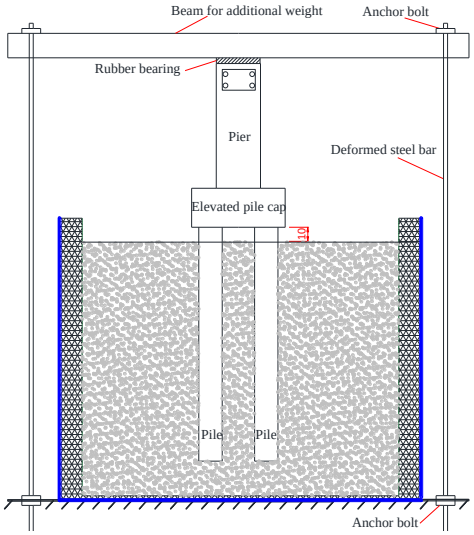

(b) Vertical loading unit

Fig. 8 Loading system for quasi-static testing

(2) Foundation soil packing and pile installation

The soil is moistened firstly (approximate 18% water content) and then kept for 24 hours to make the moisture content distribute uniformly. The high density of the foundation soil can be used to ensure the laterally loaded capacity of the model pile foundation, it has been verified by previous research (Hummadi and Hasan 2019).

Firstly, a bottom soil layer is packed and compacted to determine pile positions and dig the pile hole, then four precast-concrete piles are planted into these holes, as shown in Fig. 6(a). The next step is to pack the prepared soil into the test chamber (soil container) layer by layer, every layer should be compacted by an electric compactor, as shown in Fig. 6(b). During the pile installation process, the displacement measuring devices (PVC pipes for protection) should be installed at the designed soil layers, as shown in Fig. 6(c), the test method will be described in the following.

(3) Pier and pile cap construction

The ground surface should be levelled before pier and pile cap construction. Firstly, the concrete shuttering for pile cap is assembled and part of the pile cap concrete is casted, as shown in Fig. 7(a). Note that elevated height (10 cm) of pile cap should be guaranteed. Then the concrete shuttering for pier is assembled and the remaining concrete of the pile cap and all the concrete of the pier are casted, as shown in Fig. 7(b). After removal of concrete shuttering, the concrete curing is conducted by regular water spray, shown in Fig. 7(c).

3. Experimental design

3.1 Test apparatus

This quasi-static test is carried out at the structural laboratory of Lanzhou Jiaotong University. The test apparatus consists of a test chamber (soil container), loading system and data acquisition system. The test chamber is made of steel, its dimension is 2.5 m×2.5 m×2.5 m in length, width and depth; furthermore, a layer of 10 cm-thick foam board is clung to the inner wall of the test chamber to reduce the boundary effect. The loading system

Fig. 9 Layout of the completed model and loading system

includes lateral and vertical loading units, of which the lateral loading unit is equipped by a horizontal electro hydraulic servo jack, as shown in Fig. 8(a). The vertical loading unit consists of an H-shaped steel beam and two high-strength deformed bars with anchor bolts, it can provide vertical loading by tightening bolts, as shown in Fig. 8(b). Fig. 9 shows a layout of the completed model and loading system.

3.2 Measuring point arrangement

During testing process, the displacement of the pier-top is collected by the lateral loading unit. The lateral displacements of the pile foundation at different depth are measured by the displacement meters with bracing wires. The displacement meters are fixed at a support frame and connected to the measuring points at pile shaft by bracing wires, as shown in Fig. 8(a). To improve the measuring accuracy, PVC pipes are used as protective sleeve for these bracing wires, as shown in Figs. 6(c) and 10(a). Therefore, when the pile is subjected to lateral deformation, the brace wire will pull the displacement meter to produce same deformation, the value will be collected by the displacement meters. Strain gages are pasted on the designed positions of steel bars during reinforcement assembling, the measuring points are designed as shown in Fig. 10(b).

3.3 Loading protocol

A constant vertical load is applied on the pier top by tightening anchor bolts (Fig. 8(b)), which is the sum of the weight of superstructure (97.4 kN) and the additional

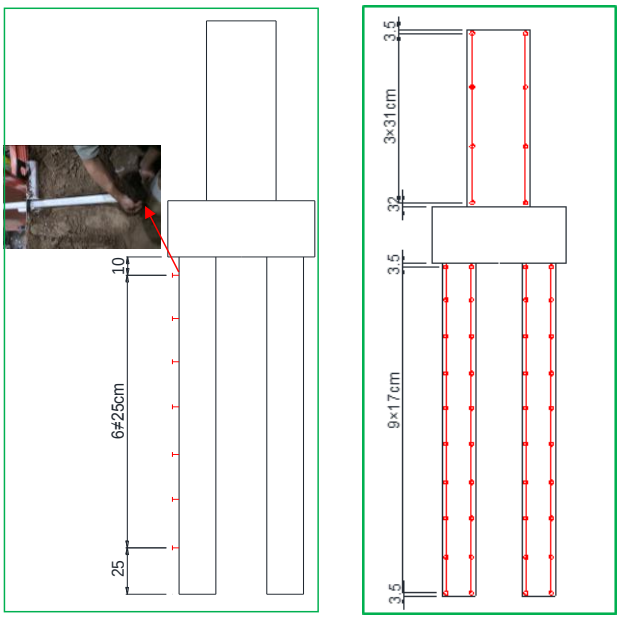

(a) Displacement measuring point (b) Steel strain measuring points

Fig. 10 Layout of the measuring point

weight (91.1 kN) in consideration of the insufficiency of the concrete unit weight due to the reduced scale. Cyclic lateral load is applied by the horizontal electro hydraulic servo jack (Fig. 8(a)) with the displacement control method, as shown in Fig. 11. The increment of a step is 2 mm before the loading displacement reaches to 10 mm, and after that an increment of 5 mm is adopted. Every loading step repeats three times, the ultimate loading displacement is 50 mm in this study.

4. Results analysis

4.1 Failure characteristics

The model pier-pile-soil system experiences initial deforming to failure stage under low frequency cyclic loading. When the loading displacement reaches to 6 mm, slight separation between the pile and surrounding soil is observed at the soil surface. The first tiny soil crack occurs at the pile side when the loading displacement increases to 8 mm. Cracks at the side of other three piles occur when the

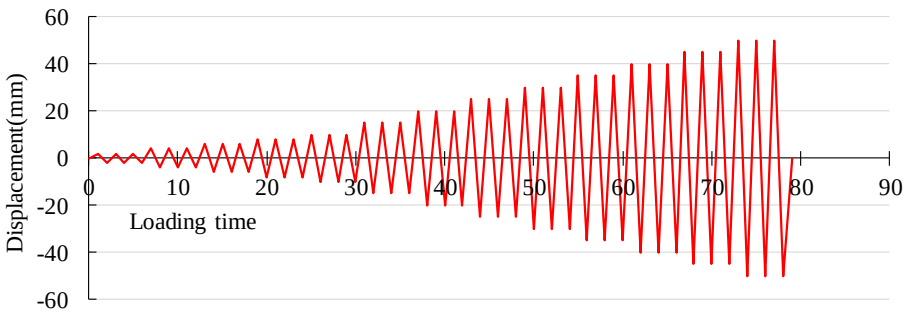

Fig. 11 Lateral loading protocol with displacement control method

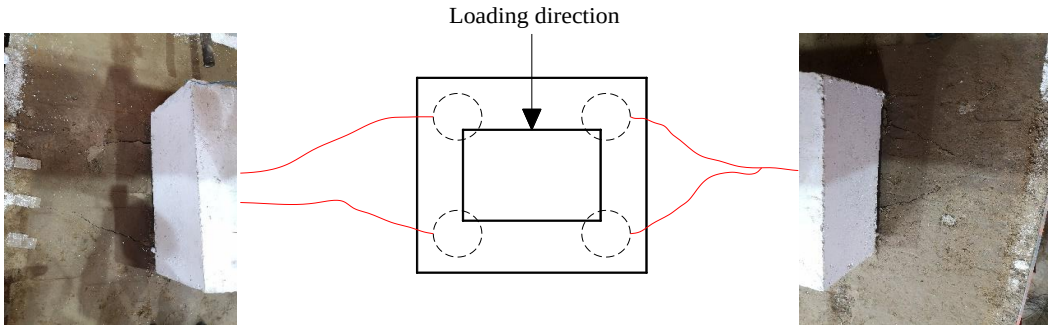

Fig. 12 Crack distributions at soil surface after testing

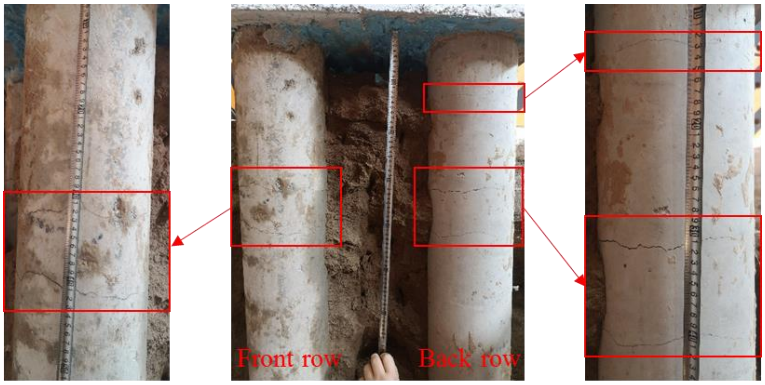

Fig. 13 Crack distributions at pile shaft after testing

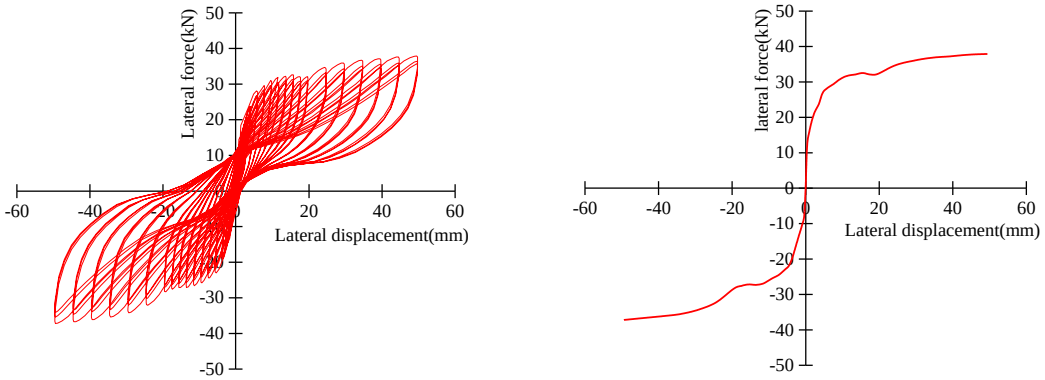

(a) Hysteretic curves (b) Skeleton curve

Fig. 14 Force-displacement relationship of the pier-top under cyclic loading

displacement reaches to 12 mm. The width and depth of these cracks increase with the increase of the lateral loading displacement. The maximum crack width is around 3-4 mm when the loading displacement increases to 20 mm. The direction trend of soil cracks close to the pile is approximately perpendicular to the loading direction. Away from the pile, the two cracks at the same side gradually converge towards to center and tend to intersect with each other eventually, as shown in Fig. 12.

In order to observe the failure characteristics of the precast-concrete pile, the surrounding soil is cleared out after testing. Fig. 13 shows the crack distributions at the front (left side in Fig. 13) and back (right side in Fig. 13) row piles, here the front row is the side with lateral loading point, back row is the opposite side (Fig. 8(a)). It can be found that main cracks exist at around 32 cm and 42 cm depths of all the piles from the bottom of pile cap, and crack with smaller width only occurs at around 12 cm-depth of the back-row pile. In this study, the elevated height is relatively small (only 0.53D, D is the pile diameter). Pile cracking regions in this study are located below the ground surface, different from an elevated pile-cap foundation with larger elevated height (more than 5D), which have most remarkable concrete cracking at the aboveground piles (Wang *et al*. 2016). Nevertheless, damage locations of elevated-cap pile foundations are sensitive to the aboveground height, group layout, soil properties and many other factors.

No cracks are observed at the bridge pier, which indicates that the pier basically keeps elastic under cyclic loading. This is due to the large cross-section of the pier, so called gravity pier (Chen *et al*. 2018) in railway bridges.

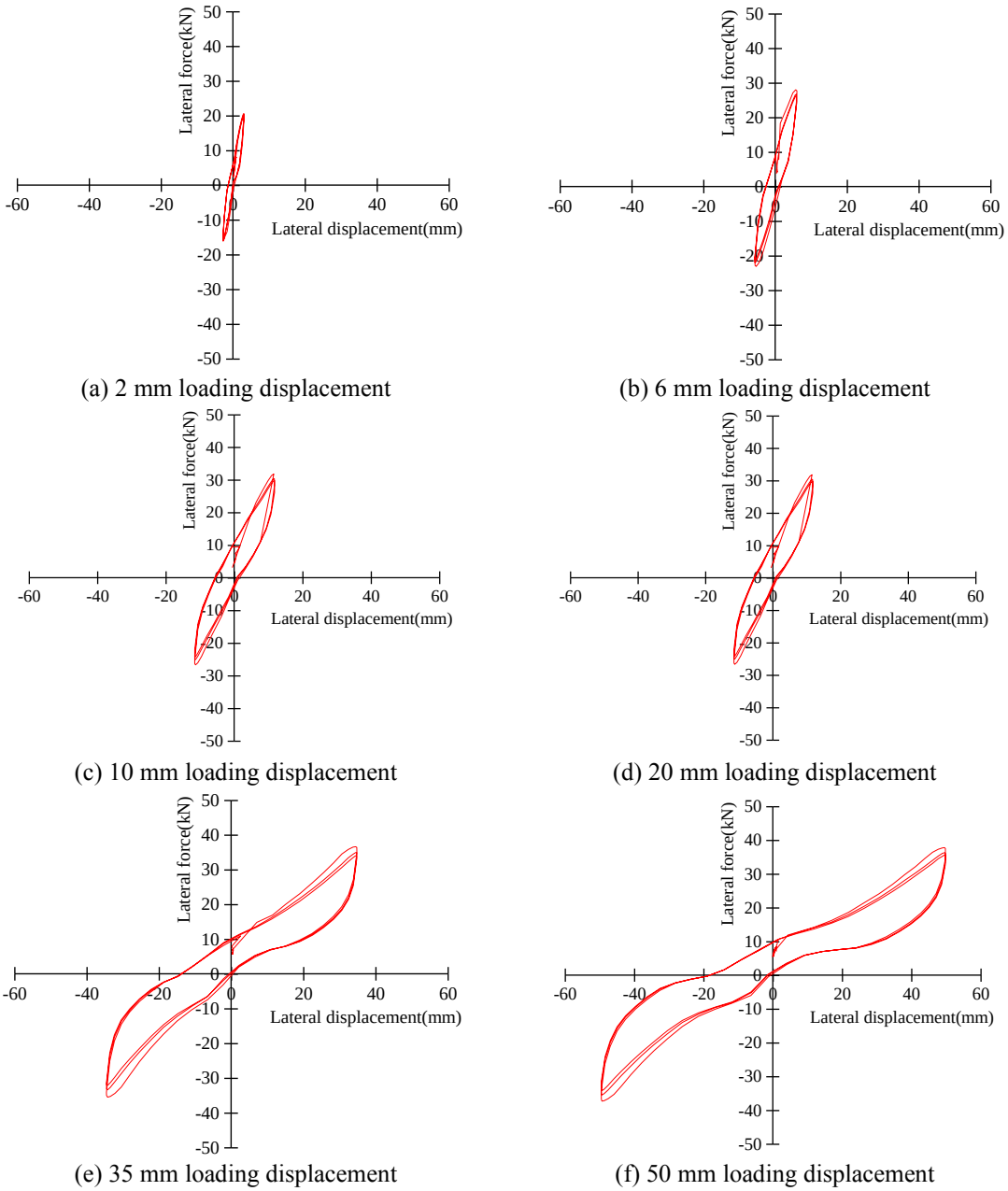

(a) 2 mm loading displacement (b) 6 mm loading displacement

(c) 10 mm loading displacement (d) 20 mm loading displacement

(e) 35 mm loading displacement (f) 50 mm loading displacement

Fig. 15 Hysteretic hoops under different loading steps

Therefore, in some cases, the seismic behavior of the railway bridge with elevated pile cap mainly depends on the response of the soil-pile interaction system. On the other hand, the gravity pier widely applied in railways most unlikely enter plastic state under earthquakes. Therefore, the lateral displacement or drift cannot be used to evaluate damage of the railway bridge pier with elevated-cap pile foundation under the seismic load, it is different from the reinforced concrete column in some seismic codes (Cansiz *et al*. 2019).

4.2 Hysteretic behavior

The lateral force-displacement relationship of the pier-top under cyclic load is recorded by the horizontal hydraulic actuator. Figs. 14(a) and (b) show the hysteretic curves and their envelope curve, also known as skeleton curve or backbone curve (Xue *et al*. 2019), respectively. It can be found that the lateral force keeps increasing with the increase of loading displacement, as seen in Fig. 14(b), there is no significant strength degradation throughout the loading process. This is attributed to the compacting soil by the increasing pile displacement. The latter increase after a slight reduction maybe reduced by the increase of loading rate, because the soil strength increases with the raise of the loading rate (Xie 2011).

Based on hysteretic curves in Fig. 14(a), hysteretic hoops under critical loading steps are picked out and plotted separately, as shown in Figs. 15(a)-(f). By contrast we find that the hysteretic hoop not only changes in size but also in shape with the increase of loading displacement. At early loading phase, the slender and steep hysteretic hoop shows

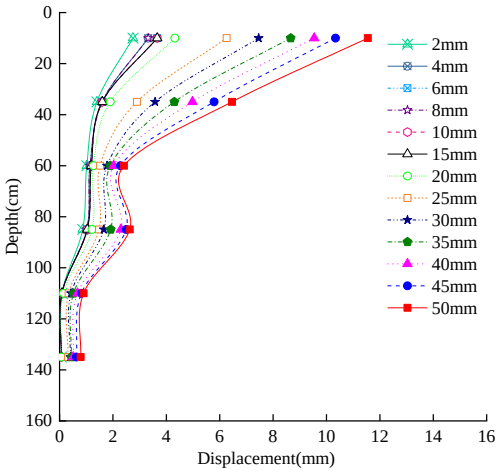

Fig. 16 Peak displacement distribution of the pile under different loading displacement

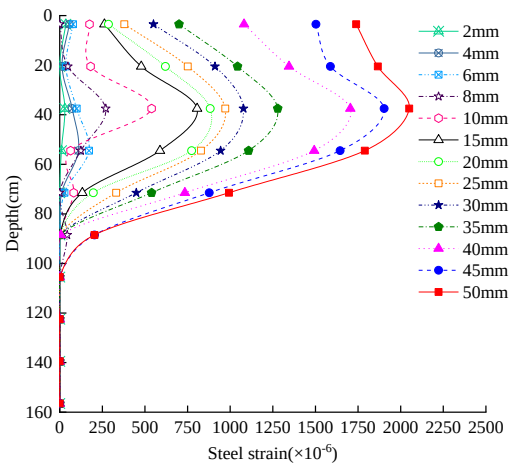

Fig. 17 Peak steel tension train of the pile under the different loading displacement

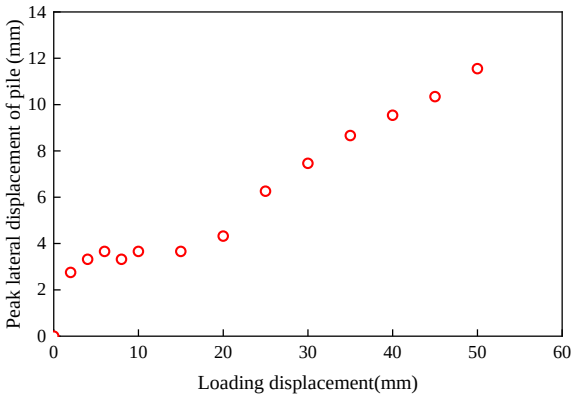

Fig. 18 The pile peak lateral displacement vs. the lateral loading displacement

a general linear elasticity of the system. With the increase of loading displacement, the hysteretic hoop becomes relatively plump and gentle, and appears obvious nonlinearity and stiffness degradation. The pinching phenomenon of the hysteretic hoop becomes more pronounced at the larger loading displacement. There are two main causes: one is related to the enlarged gap between pile and surrounding soil, another is derived from the pile uplift.

4.3 Displacement and steel strain distribution of the pile

Peak responses of piles at the positive and negative displacements for individual loading levels are plotted for analysis. The abscissa is the peak response and the ordinate is the pile depth, zero position the ordinate is the bottom of the pile cap and downward is the pile depth with positive value. Fig. 16 shows the peak lateral displacement distribution along the pile depth. Before the 20 mm of loading displacement, the lateral displacement of the pile is relatively small and increases slowly. After 20 mm of loading displacement, the lateral displacements at upper measurement points, i.e., 10 mm-depth (soil surface) and 35 mm-depth, increase rapidly with the loading displacement. However, the lateral displacement at 60 mm-depth increases extremely slowly, as a result, it is even smaller than the lateral displacement at the deeper position (measure point of 85 cm-depth). This indicates that the pile around 60cm-depth is subjected to strong soil resistance.

The steel tension train of the pile at different loading displacement is selected from measured data and plotted as in Fig. 17. As seen in Fig. 17, before 8mm of the loading displacement, the steel strain is small and the distribution characteristics of the steel train at the pile shaft are not significant. After 8 mm of the loading displacement (first soil crack occurs at this stage), it is shown that the maximum strain values occur at the range of 30-50 cm depth. Combined with the Fig. 13, it can be found that the pile cracks appear at this region precisely. The slower increase of lateral displacement at range of 35 mm-60 mm depth (Fig. 16) also indicates a stronger confining of surrounding soil for the pile foundation. Although the pile concrete is damaged, the pile reinforcements almost have no plastic deformation during the testing process. Only the maximum strain is close to yielding value under 50 mm of the loading displacement. It means that no efficient plastic hinge is formed along the pile depth. But it is worth noting that uplift of the precast pile is observed under large loading displacement due to the smoother concrete surface than cast-in-place pile. Existing research suggested that more attention should be paid to the effect of pile-uplift in seismic evaluations (Liu *et al*. 2019a).

In order to evaluate the pile uplift behavior, the relationship between the peak lateral displacement of the pile at first measured point and the loading displacement (pier-top lateral displacement) is plotted in Fig. 18. It is shown that the lateral displacement of the pile always plays a dominant role under the loading displacement (pier-top lateral displacement), the pile uplift exists but not dominates even the loading displacement becomes large.

5. Discussions

The energy dissipation can be determined by the area of

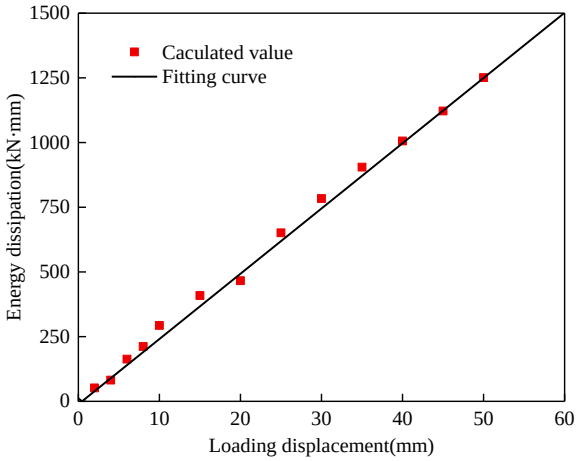

Fig. 19 Energy dissipation of the system under cyclic loading

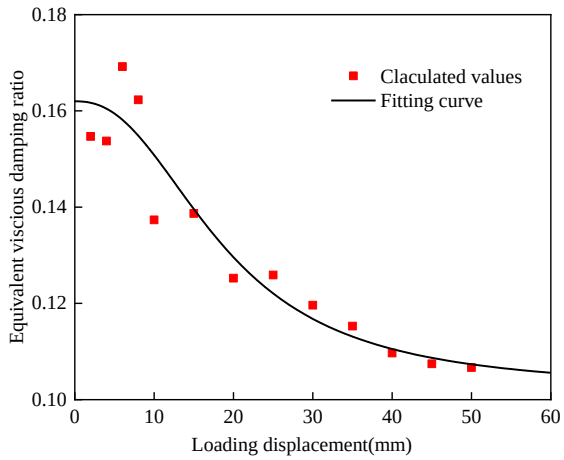

Fig .20 Equivalent viscous damping ratio of the system under cyclic loading

the hysteretic loop under cyclic loading. It can be calculated by Eq. (1) (Han *et al*. 2013).

$$\Delta W_i = \int_{u_{\min}}^{u_{\max}} \left[F_l(u) - F_{ul}(u)\right] du \tag{1}$$

Where, $F_l(u)$ and $F_{ul}(u)$ are the forces at displacement u during the loading and unloading process.

Fig. 19 shows the calculated values of the energy dissipation under different loading displacement. Apparently, the energy dissipation increases linearly with the loading displacement. The fitting curve base on the calculated values is shown in Eq. (2).

$$W = 24.99d + 11.27 \qquad R^2 = 0.997 \tag{2}$$

Where, W is the energy dissipation, and d is the loading displacement.

Test results show no damage in the gravity pier, so that the increased energy dissipation is mainly attributed by the precast pile-soil interaction system.

The equivalent viscous damping ratio ξ_{eq} can be regarded as an index of the energy dissipation capacity and is defined as Eq. (3) (Ou *et al*. 2010b).

$$\xi_{eq} = \frac{\Delta W_i}{2\pi K_{eff} \Delta_p^2} \tag{3}$$

$$K_{eff} = \frac{F_p - F_n}{\Delta_p - \Delta_n} \tag{4}$$

Where ξ_{eq} is the equivalent viscous damping ratio; ΔW_i is the energy dissipation per cycle; K_{eff} is the effective stiffness; Δ_p and Δ_n are the maximum positive and negative displacements of the hysteretic loop, respectively; and F_p and F_n are the forces at Δ_p and Δ_n, respectively.

Based on Eqs. (3) and (4), the equivalent viscous damping ratios under different loading displacement are calculated as shown in Fig. 20. It can be found that the equivalent viscous damping ratio decreases nonlinearly with the increase of loading displacement, and it tends to a stable value. As seen Fig. 19, the energy dissipation increases with the loading displacement, but it does not mean that the precast pile-soil system has higher energy dissipation capacity under larger loading displacement. Because the unyielding pile reinforcements hardly contribute to the energy dissipation, and the increase of the pile uplift with the loading displacement leads to much lower lateral resistance of pile foundations, larger cap rotation and loss of energy-dissipation capacity (Liu *et al*. 2019a). At the last stage of this test, the energy dissipation is mainly derived from the increasing lateral pile displacement in the cracked soil. Thus, the equivalent viscous damping ratio tends to stable eventually, as shown in Fig. 20.

A relation curve is presented by nonlinear fitting analysis, as shown in Eq. (5).

$$\xi_{eq} = \xi_{eqr} + \frac{\xi_{eq0} - \xi_{eqr}}{1 + \left(\frac{d}{d_0}\right)^{\alpha}} \tag{5}$$

In Eq. (5), ξ_{eq0} and ξ_{eqr} is defined as the average initial and stable residual values, they are 0.162 and 0.102 in this study, respectively; d_0 can be viewed as the threshold of loading displacement, it is 18.68 in this study; α is the fitting coefficient, it is relied on structures and loading protocol and given as 2.36 in this study.

6. Conclusions

In this study, precast concrete pile foundation with elevated cap is recommended for use for ABC of railways in regions with fragile ecological environment and adverse geological condition. A 1/8 scaled model is fabricated to investigate the failure mechanism and responses of the precast pile foundation with elevated cap under cyclic lateral loading. Some primary conclusions are drawn as following.

- Under cyclic lateral loading, main damage occurs in precast pile-soil interaction system and the bridge pier keeps in elastic state because of its relatively large cross-section. Major cracks exist at the embedded part

of the precast pile, no failure occurs at the elevated part. Soil cracks close to the pile is approximately perpendicular to the loading direction, while the two cracks at the same side tend to converge and intersect with each other away from the pile.

• Hysteretic behaviors show that there is no significant strength degradation throughout the loading process induced by the composite effect of the compacting soil and loading rate. The changing hysteretic hoop in size and shape with the increase of loading displacement reflects obvious nonlinearity and stiffness degradation of the pile-soil interaction system.

• The location of concrete cracks also has relatively larger steel strain in the precast pile, ranges from 30 to 50 cm pile depth from the bottom of the pile cap. Certainly, smaller lateral displacement at these regions of the precast pile indicates a stronger confining of the surrounding soil. No plastic hinge is formed along the pile depth, but the uplift of the precast pile is observed under larger loading displacement.

• The energy dissipation increases linearly with the loading displacement, but the equivalent viscous damping ratio decreases nonlinearly with the increase of loading displacement. Therefore, the energy dissipation capacity of the precast pile-soil system decreases with the increase of loading displacement due to the unyielding pile reinforcements and potential pile uplift.

Based on the above conclusions, it can be deduced that the precast concrete pile foundation is an available option for railway bridges in quake-prone regions with fragile ecological environment and adverse geological condition. In these regions, the precast concrete construction can effectively reduce the environmental impact, such as in permafrost, the precast-concrete pile has less thermal disturbance to the vulnerable permafrost than the cast-in-place pile accompanied by large amount of hydration heat. On the other hand, it is undeniable that there are still many problems to promote the precast concrete pile foundation in railway bridges. But there is no doubt that the research results in this study can provide a useful guidance for the accelerated bridge construction (ABC) development.

Acknowledgments

This research is supported by the National Natural Science Foundation of China (Grant No. 51808273), Project funded by China Postdoctoral Science Foundation (Grant No. 2018M643767, for Xiyin Zhang), Tianyou Youth Talent Lift Program of Lanzhou Jiaotong University (Xiyin Zhang), and lzjtu (201801) EP support. On behalf of all authors, the corresponding author states that there is no conflict of interest.

References

Ameli, M.J. and Pantelides, C.P. (2017), "Seismic analysis of precast concrete bridge columns connected with grouted splice sleeve connectors", *J. Struct. Eng.*, **143**(2), 04016176. https://doi.org/10.1061/(ASCE)ST.1943-541X.0001678.

Blanco, G., Ye, A., Wang, X. and Goicolea, J.M. (2019), "Parametric pushover analysis on elevated RC pile-cap foundations for bridges in cohesionless soils", *J. Bridge Eng.*, **24**(1), 04018104. https://doi.org/10.1061/(ASCE)BE.1943-5592.0001328.

Bu, Z., Ding, Y., Chen, J. and Li, Y. (2012), "Investigation of the seismic performance of precast segmental tall bridge columns", *Struct. Eng. Mech.*, **43**(3), 287-309. https://doi.org/10.12989/sem.2012.43.3.287.

Cansiz, S., Aydemir, C. and Arslan, G. (2019), "Comparison of displacement capacity of reinforced concrete columns with seismic codes", *Adv. Concrete Constr.*, **5**(4), 407-422. https://doi.org/10.12989/acc.2019.8.4.295.

Chen, X., Ding, M., Zhang, X., Liu, Z. and Ma, H. (2018), "Experimental investigation on seismic retrofit of gravity railway bridge pier with CFRP and steel materials", *Constr. Build. Mater.*, **182**, 371-384. https://doi.org/10.1016/j.conbuildmat.2018.06.102.

Chen, X., Zhang, X., Zhang, Y., Ding, M. and Wang, Y. (2020), "Hysteretic behaviors of pile foundation for railway bridges in loess", *Geomech. Eng.*, **20**(4), 323-331. https://doi.org/10.12989/gae.2020.20.4.323.

Cheng, Z. and Sritharan, S. (2019), "Side shear strength of preformed socket connections suitable for vertical precast members", *J. Bridge Eng.*, **24**(5), 04019025. https://doi.org/10.1061/(ASCE)BE.1943-5592.0001391.

Do, T.A., Chen, H.L., Leon, G. and Nguyen, T.H. (2019), "A combined finite difference and finite element model for temperature and stress predictions of cast-in-place cap beam on precast columns", *Constr. Build. Mater.*, **217**, 172-184. https://doi.org/10.1016/j.conbuildmat.2019.05.019.

Dziadziuszko, P. and Sobala, D. (2018), "Precast concrete piles in Europe-AARSLEFF's experience", *Proceedings of China-Europe Conference on Geotechnical Engineering*, Eds. Wu, W., and Yu, H.S., Springer International Publishing, Cham.

Fam, A., Pando, M., Filz, G. and Rizkalla, S. (2003), "Precast piles for Route 40 bridge in Virginia using concrete filled FRP tubes", *PCI J.*, **48**(3), 32-45.

Gao, Q., Wen, Z., Ming, F., Liu, J., Zhang, M. and Wei, Y. (2019), "Applicability evaluation of cast-in-place bored pile in permafrost regions based on a temperature-tracking concrete hydration model", *Appl. Therm. Eng.*, **149**, 484-491. https://doi.org/10.1016/j.applthermaleng.2018.12.097.

Gould, E. (2019), "An investigation of the structural capacity of the Alabama Department of Transportation's standard prestressed precast concrete piles", University of Alabama Libraries.

Hällmark, R., White, H. and Collin, P. (2012), "Prefabricated bridge construction across Europe and America", *Pract. Period. Struct. Des. Constr.*, **17**(3), 82-92. https://doi.org/10.1061/(ASCE)SC.1943-5576.0000116.

Han, Q., Du, X., Zhou, Y. and Lee, G.C. (2013), "Experimental study of hollow rectangular bridge column performance under vertical and cyclically bilateral loads", *Earthq. Eng. Eng. Vib.*, **12**(3), 433-445. https://doi.org/10.1007/s11803-013-0184-y.

Hummadi, O.A. and Hasan, A.M.H.M. (2019), "Effect of embedded length on laterally loaded capacity of pile foundation", *Am. Scientif. Res. J. Eng., Technol. Sci.*, **56**(1), 182-192.

Kong, B., Cai, C.S. and Zhang, Y. (2016), "Parametric study of an integral abutment bridge supported by prestressed precast concrete piles", *Eng. Struct.*, **120**, 37-48. https://doi.org/10.1016/j.engstruct.2016.04.034.

Liu, T., Wang, X. and Ye, A. (2019a), "Experimental study on seismic behavior of scoured pile-group foundations considering pile uplift", *Proceedings of Structures Congress*, 221-230.

Liu, W., Chen, L., Yu, W., Lu, Y., Yu, F. and Hu, D. (2019b),

"Experimental study on thermal performance of quicklime (CaO) energy pile aimed to thaw the warm permafrost ground", *Appl. Therm. Eng.*, **156**, 189-195. https://doi.org/10.1016/j.applthermaleng.2019.04.056.

Lu, J., Chen, X., Ding, M., Zhang, X., Liu, Z. and Yuan, H. (2019), "Experimental and numerical investigation of the seismic performance of railway piers with increasing longitudinal steel in plastic hinge area", *Earthq. Struct.*, **17**(6), 545-556. https://doi.org/10.12989/eas.2019.17.6.545.

Mashal, M. and Palermo, A. (2019), "Emulative seismic resistant technology for accelerated bridge construction", *Soil Dyn. Earthq. Eng.*, **124**, 197-211. https://doi.org/10.1016/j.soildyn.2018.12.016.

Ou, Y.C., Tsai, M.S., Chang, K.C. and Lee, G.C. (2010a), "Cyclic behavior of precast segmental concrete bridge columns with high performance or conventional steel reinforcing bars as energy dissipation bars", *Earthq. Eng. Struct. Dyn.*, **39**(11), 1181-1198. https://doi.org/10.1002/eqe.986.

Ou, Y.C., Wang, P.H., Tsai, M.S., Chang, K.C. and Lee, G.C. (2010b), "Large-scale experimental study of precast segmental unbonded posttensioned concrete bridge columns for seismic regions", *J. Struct. Eng.*, **136**(3), 255-264. https://doi.org/10.1061/(ASCE)ST.1943-541X.0000110.

Qin, Y. and Zheng, B. (2010), "The Qinghai–Tibet Railway: A landmark project and its subsequent environmental challenges", *Environ. Develop. Sustain.*, **12**(5), 859-873. https://doi.org/10.1007/s10668-009-9228-x.

Schmeisser, A.B. and Benzoni, G. (2008), "Rational seismic design of precast prestressed piles", *PCI J.*, **53**(5), 40-53. https://doi.org/10.15554/pcij.09012008.40.53.

Shang, Y., Niu, F., Wu, X. and Liu, M. (2018), "A novel refrigerant system to reduce refreezing time of cast-in-place pile foundation in permafrost regions", *Appl. Therm. Eng.*, **128**, 1151-1158. https://doi.org/10.1016/j.applthermaleng.2017.09.079.

Shim, C., Dong Lee, C. and Ji, S.W. (2018), "Crack control of precast deck loop joint using high strength concrete", *Adv. Concrete Constr.*, **6**(5), 527-543. https://doi.org/10.12989/acc.2018.6.5.527.

Sonin, A.A. (2004), "A generalization of the Π-theorem and dimensional analysis", *Proc. Nat. Acad. Sci. US Am.*, **101**(23), 8525-8526. https://doi.org/10.1073/pnas.0402931101.

Thusoo, S., Kono, S., Hamada, J. and Asai, Y. (2020), "Performance of precast hollow steel-encased high-strength concrete piles", *Eng. Struct.*, **204**, 109995. https://doi.org/10.1016/j.engstruct.2019.109995.

Titchenda Chan, K.R.M. and Zachary, B.H. (2020), "Precast seismic bridge column connection using ultra- high-performance concrete lap splice", *ACI Struct. J.*, **117**(1), 217-229. https://doi.org/10.14359/51718021.

Tong, T., Zhuo, W., Jiang, X., Lei, H. and Liu, Z. (2019), "Research on seismic resilience of prestressed precast segmental bridge piers reinforced with high-strength bars through experimental testing and numerical modelling", *Eng. Struct.*, **197**, 109335. https://doi.org/10.1016/j.engstruct.2019.109335.

Wang, J.C., Ou, Y.C., Chang, K.C. and Lee, G.C. (2008), "Large-scale seismic tests of tall concrete bridge columns with precast segmental construction", *Earthq. Eng. Struct. Dyn.*, **37**(12), 1449-1465. https://doi.org/10.1002/eqe.824.

Wang, X., Ye, A., He, Z. and Shang, Y. (2016), "Quasi-static cyclic testing of elevated RC pile-cap foundation for bridge structures", *J. Bridge Eng.*, **21**(2), 04015042. https://doi.org/10.1061/(ASCE)BE.1943-5592.0000797.

Wang, Z., Ge, J. and Wei, H. (2014), "Seismic performance of precast hollow bridge piers with different construction details", *Front. Struct. Civil Eng.*, **8**(4), 399-413. https://doi.org/10.1007/s11709-014-0273-7.

Xiao, Y., Guo, Y.R., Zhu, P.S., Kunnath, S. and Martin, G.R. (2012), "Networked pseudodynamic testing of bridge pier and precast pile foundation", *Eng. Struct.*, **38**, 32-41. https://doi.org/10.1016/j.engstruct.2011.12.020.

Xiao, Y., Wu, H., Yaprak, T.T., Martin, G.R. and Mander, J.B. (2006), "Experimental studies on seismic behavior of steel pile-to-pile-cap connections", *J. Bridge Eng.*, **11**(2), 151-159. https://doi.org/10.1061/(ASCE)1084-0702(2006)11:2(151).

Xie, D. (2011), *Soil Dynamics*, Higher Education Press, Beijing, China.

Xue, J., Zhao, X., Ke, X., Zhang, F. and Ma, L. (2019), "Numerical analysis of the seismic performance of RHC-PVCT short columns", *Adv. Concrete Constr.*, **8**(4), 295-304. https://doi.org/10.12989/acc.2019.8.4.257.

You, Y., Wang, J., Wu, Q., Yu, Q., Pan, X., Wang, X. and Guo, L. (2017), "Causes of pile foundation failure in permafrost regions: The case study of a dry bridge of the Qinghai-Tibet Railway", *Eng. Geol.*, **230**, 95-103. https://doi.org/10.1016/j.enggeo.2017.10.004.

Zhang, X., Zhang, M., Chen, X., Li, S. and Niu, F. (2017), "Effect of thermal regime on the seismic response of a dry bridge in a permafrost region along the Qinghai-Tibet Railway", *Earthq. Struct.*, **13**(5), 429-442. https://doi.org/10.12989/eas.2017.13.5.429.

CC